

# Extended cold dust emission at 1.3 mm from evolved stars

C. Sánchez Contreras<sup>1,2</sup>, J. Alcolea<sup>1</sup>, V. Bujarrabal<sup>1</sup>, and R. Neri<sup>3</sup>

<sup>1</sup> Observatorio Astronómico Nacional (IGN), Apartado 1143, E-28800 Alcalá de Henares, Spain ([sanchez,j.alcolea,bujarrabal]@oan.es)

<sup>2</sup> Departamento de Astrofísica, Facultad C. Físicas, Universidad Complutense, E-28040 Madrid, Spain

<sup>3</sup> IRAM, 300 rue de la Piscine, F-38406 St. Martin d'Hères, France (neri@iram.fr)

Received 5 March 1998 / Accepted 4 June 1998

**Abstract.** We have performed maps of the 1.3 mm continuum emission from a sample of 16 evolved stars. We have detected emission from a total of 11 objects, two of which are new detections at this wavelength: M 1-92 and, tentatively, M 1-91. 4 objects in the sample, the bipolar nebulae M 2-9, OH 231.8+4.2, NGC 7027 and CRL 2688, show extended emission in the direction of their symmetry axis up to distances from the central star  $\sim 10^{17}$  cm. We argue that most of this radio emission is arising from cold dust present in the bipolar lobes. Extended emission has not been found in the direction perpendicular to the nebular axis (except probably for NGC 7027), therefore the equatorial torus/disk of dust probably present in this type of objects is not extended enough to be detected by our observations. The 1.3 mm emission map of NGC 7027 shows an extended structure elongated approximately in the equatorial plane. This component extends up to a distance from the nebula center of about  $15''$ , and we think it could correspond to the outer region of the circumstellar disk of dust observed at shorter wavelengths in this source. In cases where extended components have been found, we estimate, assuming simplifying hypotheses, the temperature and mass of the dust. In the sources M 2-9, OH 231.8+4.2 and CRL 2688, the cold dust mass is  $\sim 2 \cdot 10^{-3} M_{\odot}$ , while NGC 7027 seems to have a larger dust content,  $\sim 10^{-2} M_{\odot}$ . For M 2-9 and OH 231.8+4.2 the uncertainty factors of our estimations have values between 2 and 3.5. For CRL 2688 the errors can be as high as a factor 10, and for NGC 7027 the dust mass given could just be a lower limit. In all the well studied cases, the cold dust component represents a large fraction of the total dust mass in the envelope ( $\gtrsim 50\%$ ) and is probably composed by relatively big grains (radii larger than  $1 \mu m$ ). We caution that the analysis of radio continuum emission can be very uncertain when not enough data on extent and spectral flux distribution exist.

**Key words:** stars: circumstellar matter – stars: AGB and post-AGB – ISM: dust, extinction – ISM: planetary nebulae: general – radio continuum: ISM – radio continuum: stars

## 1. Introduction

It is well known that stars on the red giant branch undergo a process of copious mass-loss that determines their evolution.

*Send offprint requests to:* C. Sánchez Contreras

During the subsequent evolutionary phases, the ejected material remains in the neighborhood of the central star, although subject to chemical and dynamic changes. These envelopes containing atomic and molecular gas are then characteristic of the post-AGB phases: the Protoplanetary Nebula (PPN) and the Planetary Nebula (PN) stages. In general, such nebulae also contain relatively warm dust particles that have been detected by means of their intense infrared emission. The temperature of the grains varies approximately in the range 1000–50 K. On the other hand, some post-AGB objects show spectral excesses in the millimeter range that usually have been attributed to the emission of colder dust (Walmsley et al. 1991). This cold dust component is expected to be placed in the outskirts of the nebula. Moreover, solid particles offer greater resistance than molecules to photodissociation by interstellar UV, therefore this component would better trace the outer shells of the nebula. Up to date, maps of extended radio emission from evolved objects have been practically nonexistent, so the spatial distribution and, in particular, the total extent of cold dust remained poorly known. In the case of PPNe and young PNe, it was unknown whether cold dust is concentrated in a torus/disk-like structure surrounding the central AGB star or distributed along the visible nebula. Another parameter of great importance, and equally unknown up to now, is the mass of cold dust that is present in the nebula. However, the gas-to-dust mass ratio can yield interesting information on processes of formation and destruction of grains in the circumstellar medium.

With the aim of shedding some light on the previous questions we have performed observations of the 1.3 mm continuum emission from a sample of evolved stars. Sect. 2 contains the most relevant information relative to the observational procedure. The obtained total fluxes and radio maps are also presented in this section. In Sect. 3 we describe the hypotheses and procedures followed to estimate the temperature and mass of the cold dust responsible for the millimeter emission. Finally a more detailed study of the individual objects that show extended emission is presented in Sect. 4.

## 2. Observations

We have mapped the 1.3 mm continuum emission in a selected sample of 16 evolved objects. The objects are mainly PPNe and

young PNe, but we have also included a Red Super Giant (RSG), an RV Tau star and two stars on the Asymptotic Giant Branch (AGB). All these objects are known to present extended envelopes. Data have been obtained using the MPIfR 19-channel bolometer at the IRAM-30m Radio Telescope located at Pico de Veleta (Granada, Spain). Maps were carried out in two observing runs, March 1996 and February 1997 (hereafter A and B periods respectively). The 19 elements in the multi-beam bolometer are arranged in an hexagonal lattice around a central beam. The pointing and focusing of the telescope are referred to this one. The bolometer bandpass is from 200 to 280 GHz, with the effective frequency of observation being at approximately 240 GHz ( $\sim 1.3$  mm). Details on bolometer technical specifications and instrumental calibration can be found in Kreysa (1990), Thum (1992) and Brogière et al. (1996).

Observations were made following the ON-THE-FLY standard procedure. The telescope is drifting in azimuth (with a rate of  $4''/\text{sec.}$ ) and stepping in elevation (with a scan step of  $4''$ ) while the wobbler is moving at a frequency of 2 Hz back and forth by a specific amount in azimuth. In almost all cases, we have used a wobbler throw of  $32''$ , but  $45''$  and  $62''$  have also been tried for sources with larger sizes. Double-beam maps are created by this procedure with a total azimuth size equal to the size of the array ( $100''$ ) plus twice the wobbler throw plus the expected source extent. The elevation size is of the order of the latter. Each individual map lasted from 40 to 90 minutes depending on the source size. Pointing was done before starting the maps using standard pointing sources as near as possible to the target. Calibration and focusing were made using planets (Mars and Uranus) and the intense quasar 3C273. We have also perform maps of 3C273 in order to check possible artificial beam deformations (due to the map making and reduction procedure, as well as to pointing errors). We show in Fig. 1 the resulting shape of the effective beam during A and B periods. We find that beams are significantly circular and no spurious deformations appears above the 5% contour. Therefore, we can expect that extents observed in our sources above this contour really outline the radio emission of the nebulae. The effective beam is about  $12''.3$  and  $11''.7$  for A and B periods respectively, slightly larger than the diffraction limited beam at 1.3 mm,  $11''$ . Occasionally, we had beams smaller than  $11''.7$  during period B. This was the case for the CRL 2688 map (beam  $\sim 11''.3$ ). In order to estimate the atmospheric opacity, we made sky dip scans before and after every map. Weather conditions were quite good, with zenith opacities between 0.02 and 0.2 (period B) and 0.07 and 0.4 (period A).

From a first analysis of the data obtained during period A, we found extended emission in four post-AGB objects (M 2-9, OH 231.8+4.2, NGC 7027 and CRL 2688). Such sources have also been observed during period B in order to improve the quality of our previous data. We have found quite better signal-to-noise ratio in maps carried out during period B, so we have disregarded maps from period A in these cases. Sources in our sample that showed point-like structure, were observed only during period A. An average conversion factor of  $4400 \pm 250$  Counts/(Jy/Beam) has been used for sources observed during

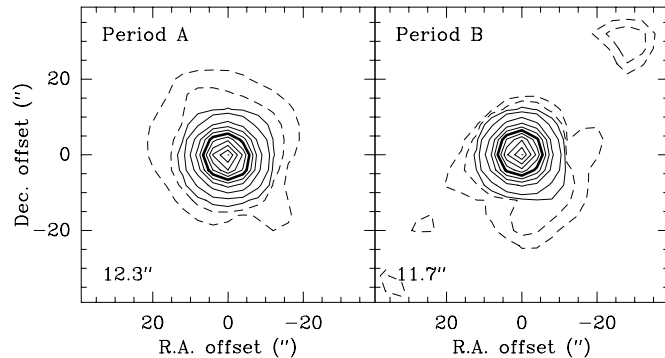


**Fig. 1.** Maps of the 1.3 mm continuum emission of a point-like object, 3C273, in periods A and B. Contours are 1.5, 3 (dashed lines), 5 and from 10 to 100 by 10% of the maximum in each epoch. A thick line has been used for the 50% contour. The corresponding FWHM is indicated in the lower-left corner.

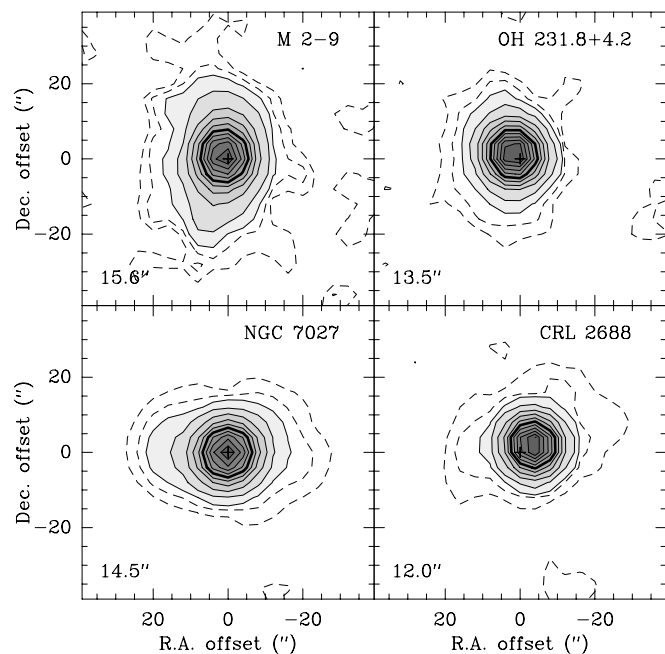


**Fig. 2.** Maps of the 1.3 mm continuum emission for extended sources obtained during period B. Contours are 1.5, 3, 5 and from 10 to 100 by 10% of the maximum in each case (M 2-9: 0.21 Jy/beam; OH 231.8+4.2: 0.56 Jy/beam; NGC 7027: 2.77 Jy/beam; CRL 2688: 1.88 Jy/beam). Levels below 5%, possibly affected by beam deformations (see text and Fig. 1), are shown by dashed lines. The 50% contour is drawn using a thick line. Values of the FWHM of the flux distribution are given in the lower-left corners.

period B, obtained from observations of our calibrators. Fluxes of the evolved objects obtained during period A have been calibrated consistently with those of period B. Data reduction was made using the NIC software package (Brogière et al. 1996).

A list of the observed sources, coordinates, total measured 1.3 mm flux and source type is presented in Table 1, together with the fluxes obtained for calibrators during period B. We have clearly detected radio continuum emission from 10 sources, and

**Table 1.** 1.3 mm total continuum flux from the observed sources.

Source	$\alpha(1950)$ ( <sup>h</sup> <sup>m</sup> <sup>s</sup> )	$\delta(1950)$ ( <sup>°</sup> <sup>'</sup> <sup>''</sup> )	$S_{1.3\text{mm}}$ (mJy)	Type
CRL 618	04 39 34.0	36 01 16	2250 ± 100	PPN
Red Rectangle	06 17 37.0	-10 36 52	230 ± 25	PPN
NGC 2346	07 06 49.7	-00 43 29	< 20	Young PN
VY CMa	07 20 54.7	-25 40 12	770 ± 40	RSG
OH 231.8+4.2	07 39 58.9	-14 35 43	715 ± 15	PPN
Frosty Leo	09 37 11.6	12 12 31	< 7	PPN
W Hya	13 46 12.2	-28 07 07	200 ± 25	AGB
M 2-9	17 02 52.6	-10 04 31	360 ± 10	Young PN
89 Her	17 53 24.0	26 03 23	< 24	PPN
R Sct	18 44 48.7	-05 45 35	< 6	RV Tau star
M 1-91*	19 30 54.9	26 46 13	30 ± 20	PPN
M 1-92	19 34 19.7	29 26 05	120 ± 20	PPN
CRL 2688	21 00 19.9	36 29 45	2100 ± 100	PPN
NGC 7027	21 05 09.4	42 02 03	3920 ± 90	Young PN
R Aqr	23 41 14.2	-15 33 42	75 ± 15	AGB, Symbiotic
M2-56	23 54 06.6	70 31 31	< 10	PPN
Calibration Sources				
3C 273	12 26 33.2	02 19 43	19 10 <sup>3</sup>	Quasar
Uranus	–	–	34 10 <sup>3</sup>	Planet
Mars	–	–	950 10 <sup>3</sup>	Planet

\*: Tentatively detected

also probably from M 1-91. So, we have found 2 new detections, M 1-92 and M 1-91. In Fig. 2 we can see the maps obtained after data reduction for M 2-9, OH 231.8+4.2, NGC 7027 and CRL 2688, the sources where we find extended 1.3 mm emission. In the lower-left corner we give an average of the FWHMs of the flux distribution in the direction of the axis of the nebula and the perpendicular one. Note, that in all cases we find this value larger than the measured beam (see above).

### 3. Temperature and mass of the dust

As we have mentioned, the 1.3 mm continuum emission in PPNe could present a contribution from a cold dust component. Of course, there is probably a continuous temperature gradient in the nebula, therefore to distinguish between cold and warm dust components is only a useful concept for the present analysis. We have estimated the total cold dust content in objects that show extended 1.3 mm emission (M 2-9, OH 231.8+4.2, NGC 7027 and CRL 2688). First, we have considered the possible contamination of the observed flux by another kind of emission mechanisms. It is known that ionized regions surrounding certain evolved stars contribute with free-free emission to the radio continuum. In cases where the electron density distribution is assumed to be constant, the radio spectrum varies as  $\nu^{-0.1}$  for optically thin and as  $\nu^2$  for optically thick HII regions (e.g. Mezger et al. 1967). However, in the case of electronic densities varying as  $r^{-2}$  (for instance in nebulae resulting from spherical mass ejections with constant mass-loss rates) the radio spectrum is found to vary as  $\nu^{0.6}$  (Panagia and Felli 1975). Also, some contamination by molecular lines, stellar photosphere and even warm dust emission could exist. In Sect. 4, the contribution of these different emission mechanisms to the measured 1.3 mm

flux has been considered and subtracted, if necessary, for the individual sources.

The remaining flux is then only arising from cold dust. We have assumed that at this relatively long wavelength the nebular dust is optically thin, therefore the flux is proportional to the opacity,  $\tau$ , that can be expressed as

$$\tau = N_d \pi a^2 Q_\nu(a) \quad (1)$$

Here  $N_d$  is the column density of dust,  $a$  is the grain radius and  $Q_\nu(a)$  is the grain emissivity that we suppose depends on frequency and grain size in the form:

$$Q_\nu(a) = \begin{cases} (\nu/\nu_0)^\alpha & \text{if } \nu < \nu_0 \\ 1 & \text{if } \nu > \nu_0 \end{cases} ; \nu_0 = c/4\pi a \quad (2)$$

where  $c$  is the light speed. Dust emissivities following a power-law have been previously obtained empirically in cool molecular clouds and in envelopes of late type stars (Schwartz 1982; Bussoletti et al. 1987 and references therein).  $\alpha$  and  $\nu_0$  are known to depend on the composition and size of the grains,  $\alpha \sim 1$  being indicative of amorphous carbon grains or large particles with impurities or mantles, whereas  $\alpha \sim 2$  is usually associated to crystalline structures (Rowan-Robinson 1986; Gilman 1974; Leung 1975). The emissivity law has  $\alpha = 1$  in the frame of the Mie theory, i.e for spherical conducting particles of uniform composition with radius smaller than the wavelength of the incident radiation ( $a \ll \lambda$ ). We will consider in the following that  $\alpha$  ranges between 1 and 2.

Assuming that grains emit like modified black-bodies, we find that the total dust mass,  $M_d$  ( $M_\odot$ ), is given by

$$M_d = 3 \cdot 10^{-14} S_{1.3 \text{ mm}} (e^{11.66/T_d} - 1) \rho D^2 a / Q_{1.3 \text{ mm}}(a) \quad (3)$$

**Table 2.** Flux of the detected extended cold dust components. The allowed dust temperature range, the spectral index obtained from the spectral fit and the assumed grain radius range are also shown in columns 3, 4 and 5. Columns 6, 7 and 8 contain, respectively, the distance to the source, its luminosity and references for them. In column 8 the calculated mass of cold dust in the nebula and its uncertainty factor (brackets) are shown. The asterisk (\*) denotes particularly uncertain values, see Sects. 4.3 and 4.4. For CRL 2688 the results correspond to the whole dust envelope.

Source	$S_{1.3\text{mm}}^{\text{cd}}$ (mJy)	$T_{\text{cd}}$ (K)	$\alpha$	$a$ ( $\mu\text{m}$ )	$D$ (pc)	$L$ ( $L_{\odot}$ )	Ref.	$M_{\text{cd}}$ ( $M_{\odot}$ )
M 2-9	$150 \pm 10$	25-5	1-2	1-100	650	550	Schwarz et al. (1997)	$1.5 \cdot 10^{-3}(3.5)$
OH 231.8+4.2	$165 \pm 15$	40-15	1	10-100	1500	10000	Sánchez Contreras et al. (1997)	$2.0 \cdot 10^{-3}(2.0)$
NGC 7027	$300 \pm 90$	10-30	2	5-20	1000	10000	Middlemass (1990)	$3.5 \cdot 10^{-2}(*)$
CRL 2688	$2100 \pm 100$	115-40	0.7	0.2-1000	1000	20000	Knapp et al. (1993)	$2.0 \cdot 10^{-3}(*)$

where  $S_{1.3\text{ mm}}$  and  $Q_{1.3\text{ mm}}(a)$  are, respectively, the measured flux in mJy and the grain emissivity at 1.3 mm,  $T_{\text{d}}$  is the dust temperature in K,  $D$  is the distance to the source in pc,  $\rho$  is the grain density in  $\text{gr cm}^{-3}$  and  $a$  is the grain radius in  $\mu\text{m}$ .

Unfortunately our knowledge of the properties and physical conditions of dust grains is very poor. There is a great variety of possible values of size and density of the grains present in nebulae surrounding evolved objects. In general radii ranging from  $\sim 0.01$  to  $\sim 20 \mu\text{m}$  are commonly accepted as possible sizes (e.g. Hildebrand 1983). However, larger grains ( $a \geq 200 \mu\text{m}$ ) have been proposed in order to explain the continuum excess in the millimeter and centimeter spectral ranges (Jura et al. 1997). Since the grain size has a great influence on dust mass calculation, we have taken into account several cases. As we will explain later, we can use the information extracted from our observations (dust temperature and map extent) to minimize the interval of possible dust radii. The density of the grains, depends on their (unknown) chemical composition, but we will suppose that it does not significantly separate from  $3 \text{ gr cm}^{-3}$ , that is a relatively good average value for both Carbon and Oxygen containing particles (Hildebrand 1983).

The dust temperature and the power-law index of the grain emissivity,  $\alpha$ , have been simultaneously estimated fitting the millimeter spectrum with a function of the type:

$$F_{\nu} \propto B_{\nu}(T_{\text{d}}) \nu^{\alpha} \quad (4)$$

with  $B_{\nu}(T_{\text{d}})$  being the Planck function. In general, it is not possible to make a good fit of the total spectral energy distribution using a single isothermal dust population. In most cases, there is a widening of the spectrum that clearly indicates the presence of a temperature gradient in the nebula. However, it is possible to establish from the fit an upper and a lower limit to the temperature of the coldest grains, in which we are interested. The whole range will be considered in our calculations. Also, the temperature of the warmer grains has been obtained using the same procedure. The spectral index,  $\alpha$ , has been estimated, as we have mentioned, from the fit of the spectrum. In most cases, the millimeter excess does not allow a proper estimate of this index for the cold dust component. Therefore, we have used in this case the same value of  $\alpha$  that we obtained for the warm dust component. However, we must note that colder grains could have a different composition and structure and, subsequently, a different value of  $\alpha$ . In Sect. 4 these other possibilities are discussed individually for the extended sources.

As we have previously mentioned, there is a relatively simple way to estimate the grain radius from our data. Once we have subtracted any other possible contribution to the flux, we can measure from our maps the total extent of the emission arising from grains at a representative temperature,  $T_{\text{d}}$ , obtained from the fit of the spectrum. In other words, we know the dust temperature (from the spectral fit) at a given distance of the nebula center (from the maps). On the other hand, we can theoretically calculate the temperature as a function of the distance to the central star. To do this we have supposed that radiative equilibrium holds in the nebula dust, i.e. the energy absorbed by grains is totally reemitted at longer wavelengths, and that the only mechanism of heating grains is radiation from the star. Due to the relatively high temperature of the star, we have assumed such radiation mostly concentrated in the optical spectral range, where grains have a flat emissivity law. We are also assuming that scattering is negligible in this spectral region, so extinction is given only by the absorption coefficient. Taking into account the previous simplifying assumptions the dust temperature can be expressed as:

$$T_{\text{d}} \propto \left( \frac{L}{r^2 a^{\alpha}} \right)^{\frac{1}{\alpha+4}} \quad (5)$$

where  $r$  is the distance of the dust from the nebula center and  $L$  the stellar luminosity. The extinction of dust placed between the central star and the grains we are considering is not explicitly shown in that equation. Such an effect can be introduced in a straightforward way, and has been taken into account in some of the studied sources.

Eq. (5) shows that the temperature distribution so determined depends on the grain size. Only certain values of this parameter are then compatible with a temperature  $T_{\text{d}}$  at the observed distance. The comparison between the theoretical temperature distribution and the temperature from the spectral fit, taken into account the distance obtained from the map, is so used to shorten the previous interval of possible grain radii.

We must note from Eqs. (3) and (5) that the mass calculated under the previous hypotheses explicitly varies with the assumed distance to the source, as  $D^2$ , and implicitly through the dust temperature and the grain radii. However, both  $L$  and  $r^2$ , are proportional to  $D^2$ , so the determination of the grain temperature and radius at a given angular distance from the central star is not affected by  $D$  (Eq. [5]). Therefore, the only depen-

dence of the mass on the distance to the source is as  $D^2$  due to the factor in Eq. (3).

#### 4. Individual sources

In this section we discuss in detail sources for which we find that the full width at half maximum (FWHM) of the flux distribution is larger than the telescope beam size (Sect. 2). For these objects, we have made a decomposition of the flux in several components. In all these cases, we have found a spatially unresolved component, which has been fitted by a two-dimensional gaussian function (with maximum intensity and width equal to that of the telescope beam) and subtracted from the total flux. Note that the flux from the remaining component is then a lower limit. This remaining emission is extended and, usually, elongated along the nebula axis. We have applied to these sources the procedure explained in Sect. 3 in order to estimate the dust content of this extended region. Results on the cold dust component ( $T_{\text{cd}}$ ,  $\alpha$ ,  $a$  and  $M_{\text{cd}}$ ) are shown in Table 2.  $M_{\text{cd}}$  in Table 2 is our best estimate, we also give between brackets an estimated uncertainty. In the next four subsections we present the calculation details for the extended sources. Sect. 4.5 is dedicated to describe our results on point-like objects.

##### 4.1. M 2-9

M 2-9 is classified as a young PN by virtue of its strong bipolar appearance in the visible and also at longer wavelengths (Kohoutek & Surdej 1980; Kwok et al. 1985 and Aspin et al. 1988) and of the position of its central star in the H-R diagram. This is confirmed by the detection of CO emission from the remnant of the past AGB envelope (Bachiller et al. 1988; Zweigle et al. 1997) that originates in a small inner torus with a diameter  $\sim 6''$ . The brightest nebulosity associated to this object has an extent of about  $40''$  along the nebula axis (approximately in the North-South direction), and there are also two fainter collimated outflows reaching a total extent of  $115''$  in the same direction. M 2-9 is characterized by intense IR emission arising from different dust components. According to Allen & Swings (1972), warm dust with temperature  $\sim 800$  K is present in a compact region surrounding the central star. Moreover, high resolution IR images of M 2-9 taken by Aspin et al., show that there is a highly reddened disk-like feature that extends about  $20''$  in the East-West direction across the central core. Recently, Schwarz et al. (1997) have shown from observations of scattering in the visible, that there is also dust lying on the farthest faint loops. On the other hand, the millimeter emission excess observed in M 2-9 could indicate also the existence of a cold dust component in the nebula.

From our data, M 2-9 presents a total integrated 1.3 mm flux of  $360 \pm 10$  mJy. After subtraction of a central compact component with a flux of  $\sim 210$  mJy, it remains an extended component lying in the direction of the nebula axis with a flux of  $\sim 150$  mJy (Fig. 3a). We can see in this figure that the emission appears clearly separated in two components, associated to the bright lobes of M 2-9. Two maxima are present in the map lo-

cated at about  $12''$  toward the North and the South respectively. The southern maximum is displaced toward the East approximately  $4''$ . In the direction perpendicular to the nebula axis, the extent of the emission from the lobes is  $\sim 12''.5$  after deconvolution with the telescope beam size. The contribution of the photospheric emission and the molecular lines (see Zweigle et al.) to the compact flux of M 2-9 is negligible. Note that the CO emission from this source and, consequently, the whole molecular emission, is known to be spatially compact and anomalously weak, due probably to molecular photodissociation.

In Fig. 3b we show the spectral energy distribution. The contribution to the flux at small wavelengths of thermal dust emission is remarkable. The relatively large width of the spectrum in this range indicates the existence of a temperature gradient in the nebula. We have found, from the spectral fit, grains having temperatures between 800 K and 70 K with  $\alpha = 1$  (see e.g. short-wavelength data from Allen & Swings). Note that this warm dust component, that already have a low value of  $\alpha$ , can not explain the 1.3 mm observed flux.

At larger wavelengths free-free emission becomes important. At this spectral range, there are two emission components. It seems well known from previous radio continuum observations (Purton et al. 1975; Kwok et al.; Zweigle et al.), that there is an extended emission component arising from homogeneous HII regions located in the lobes, which follows a frequency law  $\propto \nu^{-0.1}$  and, therefore, does not contribute a lot to the total 1.3 mm flux. Also, it exists a very compact component of emission in the nebula center, identified in VLA observations, arising from an ionized stellar wind that leads to a spectrum rising as  $\nu^{0.6}$ . In fig. 3b both the emission from the compact component (triangles) and the total flux (circles), which at large wavelengths equals that of the extended component, are shown. We have found that at least two different  $\nu^{-0.1}$  free-free components are needed to properly fit the 6 and 20 cm data. However, the dispersion of the points in this part of the spectrum makes difficult to decide about the best fit. Anyway, the spectral fitting at these wavelengths have little influence on the analysis of the mm-wave continuum due to the low free-free emission of the extended ionized gas at 1.3 mm.

It is clear from the spectrum in Fig. 3b, that it is not possible to reproduce the observed millimeter continuum flux taking only into account the emission from warm dust and from the ionized gas. We have tried to separately fit the spectrum associated to the compact (triangles, Fig. 3b) and the extended (squares) emission from M 2-9. The flux from the warm dust plus the core wind emission (dashed line), explains the observed 1.3 mm flux from the central compact region. However, the extended free-free emission from the lobes,  $\sim 40$  mJy in the millimeter range, is not enough to explain the extended component in our observations. The most probable explanation to the millimeter excess, as previously suggested by several authors, is the presence of cold dust in the nebula. The total emission from all these components is represented in Fig. 3b by the solid line.

We have fitted the contribution of this extended cold dust using the procedure described in Sect. 3. From the spectral fit we have found temperatures in the range 25 to 5 K for the coolest

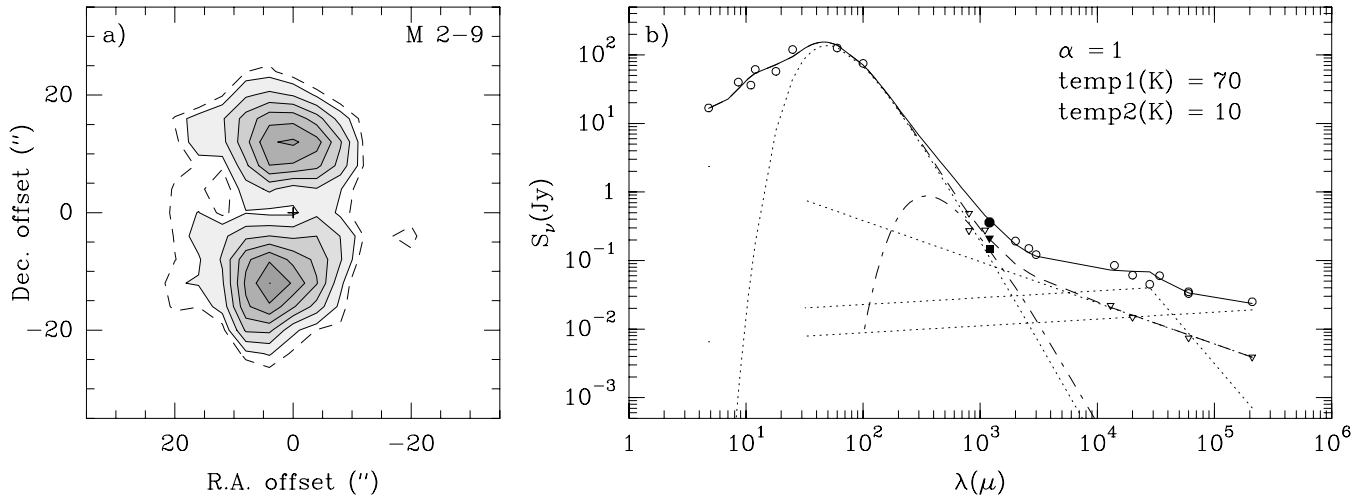


**Fig. 3.** **a** Map of the extended component of M 2-9, after subtraction of a compact component to the total 1.3 mm emission. Contours are 18 (dashed line) and from 25 to 100 by 12.5% of the maximum (36 mJy/beam). The dashed contour could present artificial deformations (Sect. 2). **b** Spectral energy distribution of the source. Filled symbols represent 1.3 mm data from this work; error bars are too short to be represented. Triangles are used for the flux associated to the compact component, in the centimeter range they correspond to high resolution VLA data from Kwok et al. (1985), and in the submillimeter range to data from observations with telescope beams smaller than the source extent (Hoare et al. 1992). We use the square for our extended component, and circles for the total emission from observations with telescope beams covering the whole nebula, see Zijlstra et al. (1989), Purton et al. (1982), Gezari et al. (1987), Beichman et al. (1988), Zweigle et al. (1997), and Milne & Aller (1982). Dot-dashed line: thermal cold dust emission (10 K); dotted lines: free-free and thermal warm dust emission (70 K); dashed line: model fit to the compact component; solid line: model fit to the total emission, (see text for details on model fitting). Note that the fit of the spectrum at small wavelengths has been done also using two other warm dust components of 550 and 200 K.

component (dash-dotted line, Fig. 3b). Looking at the 1.3 mm map in Fig. 3a, we can see that dust at the temperature previously estimated must exist at  $\gtrsim 12''$ . In order to calculate the cold dust mass in the nebula, we have considered several possible situations, i.e. values of the grain radius and spectral index which theoretically (Sect. 3) reproduce the temperature from the spectral fit at the observed distance on the map. Following this procedure it is deduced that grains must be  $\gtrsim 1 \mu\text{m}$ , either for  $\alpha = 1$  or  $\alpha = 2$ . First, using a value of  $\alpha = 1$ , we have found that radii between  $1.5\text{-}20 \mu\text{m}$  lead to temperatures at  $\sim 12''$  between 25-15 K. The resulting mass is  $M_{\text{cd}} \sim 4.4 \cdot 10^{-4} M_\odot$ . With a value of  $\alpha = 2$ , grains with radii between  $4\text{-}20 \mu\text{m}$  lead to temperatures between 25-14 K. The obtained mass in this case is  $M_{\text{cd}} \sim 5.3 \cdot 10^{-3} M_\odot$ . So, we have found an average value of  $M_{\text{cd}} \sim 1.5 \cdot 10^{-3} M_\odot$  with an uncertainty factor 3.5. It is remarkable that only in the case of having grains with sizes  $\gtrsim 100 \mu\text{m}$  it is possible to reach temperatures as low as 5-10 K at  $12''$  from the nebula center. For these unexpectedly high radii we estimate the cold dust component to have a mass  $M_{\text{cd}} \sim 1.2 \cdot 10^{-3} M_\odot$ , not very different from the mass values found above (note that in this case this value is not dependent on  $\alpha$ ).

We have also estimated the effects on our calculations of a certain opacity between the central star and the studied cold grains. For  $A_v=1$ , which is almost an upper limit in the lobes direction, we find that grain radii as small as  $0.6 \mu\text{m}$  are allowed and that the temperature can range between 25 and 10 K. The cold dust mass estimated under these conditions has similar values as in the previous cases.

From the spectral fit, we have also estimated the flux from the warm dust component,  $\sim 110$  mJy, and its mass. We have found a value of  $M_{\text{wd}} \sim 7.8 \cdot 10^{-5} M_\odot$ . We can compare the dust content in the nebula with the molecular and ionized mass estimated by other authors. Kwok et al. estimated the ionized mass  $\gtrsim 10^{-2} M_\odot$ . On the other hand, Zweigle et al. give a value of the total molecular mass  $\gtrsim 4 \cdot 10^{-3} M_\odot$  (rescaling their results to our distance to the source).

No emission from dust in the faint lobes (at distances to the nebula center greater than  $20''$ ) have been found. This fact is very probably due to the low mass content in these regions (between  $1.1 \cdot 10^{-3}$  and  $5.6 \cdot 10^{-3} M_\odot$ , from Schwarz et al.).

Note the position agreement of the maxima on the 1.3 mm map with those in the 6 cm map from free-free emission (Bowers & Knapp 1989). This fact is not so surprising even if the extended component arises from cold dust. Actually, the maxima in our map also approximately agree with some of the bright knots observed in the visible. It seems that the regions located on the emission maxima are really mass condensations.

As we have mentioned in Sect. 3, the estimated dust mass depends on the distance to the source as  $D^2$ . We have assumed for M 2-9 a relatively low value of such a parameter from calculations by Schwarz et al. (1997). However, the distance to this source has been usually assumed to be larger,  $\sim 1000$  pc, the mass estimated in this case being  $\sim 2.4$  times larger.

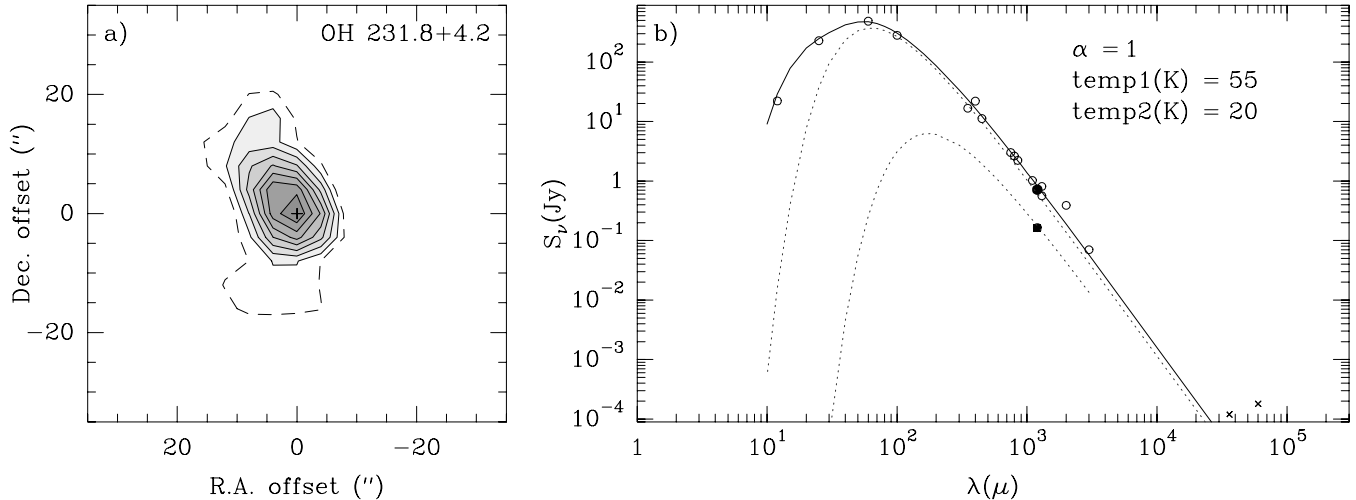


**Fig. 4.** **a** Map of the extended component of OH 231.8+4.2. Contours are 20 (dashed) and from 30 to 100 by 10% of the maximum (88 mJy/beam) **b** Spectral energy distribution of the source. Filled symbols represent our 1.3 mm data. Circles correspond to the total emission from the source (Knapp et al. 1993; Sopka et al. 1985; Walmsley et al. 1991 and IRAS Point Source Catalogue), crosses are flux upper limits (Bowers & Knapp 1989; Knapp et al. 1995) and the square corresponds to our extended component. Dotted lines: thermal dust emission from warm (55 K) and cold (20 K) components; solid line: model fit of the total emission from the source. For the short waves we have also included a 120 K dust component.

#### 4.2. OH 231.8+4.2

OH 231.8+4.2 is one of the best studied PPN due, in part, to its relative proximity ( $\sim 1500$  pc, Bowers & Morris 1984; Kastner et al. 1992) and large extent. Its optical image shows a clear axial symmetry (Reipurth 1987), with two reflection lobes, two collimated jets and an obscuring ridge surrounding the central star, a Mira variable classified M9 III (Feast et al. 1983; Cohen et al. 1981). OH 231.8+4.2 has a very extended and massive envelope, reaching  $\sim 50''$  in the axial direction and containing a total mass between 0.5 and  $1 M_{\odot}$  (Sánchez Contreras et al. 1997). Observations at infrared wavelengths indicate the presence of dust in the nebula, both distributed along the bipolar lobes and in the disk surrounding the central star (Kastner et al. 1995). Several spectral features in the NIR have been detected and attributed to water ice and cold silicate grains ( $T \lesssim 100$  K) (Soifer et al. 1981; Gillet et al. 1976). However, the presence of colder solid particles in OH 231.8+4.2 is suggested by the millimeter excess found in its energy distribution.

We have separated the total millimeter emission from OH 231.8+4.2,  $715 \pm 15$  mJy, in two components, a compact component of about 550 mJy and an extended component of, at least, 165 mJy. The latter, that can be seen in Fig. 4a, is lying along the direction of the nebula axis with a total extent  $\lesssim 20''$ . The size of the 50% contour in this direction is  $\sim 16''$ , so we deduce a total extent for the emission  $\sim 11''$ . It seems that the 1.3 mm emission extends up to somewhat larger distances from the center in the northern lobe than in the southern one. The same distribution is observed in NIR maps (Woodward et al. 1989; Shure et al. 1995; Kastner et al. 1995). A small structure at approximately  $+6'', +13''$  (R.A. and Dec. offsets from the center) can be seen in our map. This feature is coincident with the northern Herbig-Haro object observed in the visible (Cohen et

al. 1985) as well as with the relative maximum observed in  $H$  and  $K$  bands (Woodward et al.) and in CO maps (unpublished data).

The spectral energy distribution of OH 231.8+4.2, clearly indicates that thermal dust emission is the dominant mechanism in the nebula. No evidence of free-free emission has been found up to now and the contributions to the flux from photospheric or line emission are negligible,  $\lesssim 5\%$ . The spectrum of OH 231.8+4.2 can be well fitted between 20 and  $100 \mu\text{m}$  by dust thermal emission with a single temperature between 75 and 100 K using an emissivity frequency law with  $\alpha = 1$ . However, this relatively warm dust component does not explain the observed flux at wavelengths larger than  $400 \mu\text{m}$ . To fit the whole spectrum, colder components must be considered. The FIR and submillimeter emission is well fitted introducing dust at 55 K with  $\alpha = 1$  (see Fig. 4b). Moreover, in view of the remaining millimeter excess it must be also a colder dust component. In order to reproduce the observed millimeter flux, we have tried several spectral fits taking into account the presence of colder grains. Looking at the spectrum of OH 231.8+4.2 we can see that the emission in the millimeter range seems to be in the Rayleigh-Jeans limit. We have established a lower limit of the temperature taking into account this fact ( $T_{\text{cd}} > h\nu/k = 11$  K). Moreover, from the theoretical temperature distribution we find that temperatures smaller than 10 K are only reached at distances to the center around  $9''$  if grains are big in excess ( $a \gtrsim 1000 \mu\text{m}$ ). Then, we have not considered in our calculations temperatures below 10 K. In order to better determine the temperature of cold grains we have also fitted the flux of our extended component. In other words, we require that the extended flux we have obtained can be reproduced by thermal emission from cold particles. Then, we have estimated a variation range of the temperature between

40 and 15 K assuming also  $\alpha = 1$  for the cold dust component. Taking into account these values we have calculated the mass of cold dust in the nebula, which is between  $1 \cdot 10^{-3}$  and  $4 \cdot 10^{-3} M_{\odot}$ . Note, that if  $\alpha = 1$  the mass does not depend on the grain radius, however, we can make some estimation of this parameter also in this case. We are assuming that the compact emission arises from the warm dust component ( $\geq 55$  K), so from the theoretical temperature distribution we can rule out grain sizes which lead to 55 K at distances to the source center larger than  $2''$ . We have accordingly found that the grain size must be  $\gtrsim 5 \mu m$ .

We have also considered for the cold component a spectral index  $\alpha = 2$ . Then, the spectral fit suggests temperatures between 15 and 5 K for this component. Grains that allows such low temperatures at the observed distances are always  $\gtrsim 100 \mu m$ , indicating a cold dust mass  $\sim 5 \cdot 10^{-3} M_{\odot}$  ( $a = 100 \mu m$ ) and increasing proportionally to  $a$ . However, larger grains are unexpected in view of the OH 231.8+4.2 spectrum. In fact, radii larger than  $100 \mu m$  have a flat emissivity law at wavelengths smaller than  $\sim 1200 \mu m$ , which is not compatible with the energy spectral distribution.

On the other hand, we have also made an estimation of the warm dust content of the nebula, assuming temperatures between 75 and 55 K. We find values for this quantity  $\sim 2\text{-}3 \cdot 10^{-3} M_{\odot}$ . So, the total content of dust in the nebula is of the order of  $5 \cdot 10^{-3} M_{\odot}$  with an uncertainty factor about 2. This value reasonably agrees with that found by Kastner et al. (1995) from the analysis of the scattered light by grains in the lobes. So, the total absorbing and scattering dust masses are similar. Following these authors, in this object a great part of the dust seems to be located at the lobes of the nebula instead of in the circumstellar disk. Our results, that shows that the 1.3 mm emission is elongated in the axial direction, support this idea. We have then found that the mass in the lobes is at least of the same order or even greater than the mass in the compact component. On the other hand, we can compare the total molecular mass in the OH 231.8+4.2 nebula with the dust mass in order to obtain the gas-to-dust ratio in this object. Sánchez Contreras et al. (1997) estimates a mass of nebular material about  $0.5\text{-}1 M_{\odot}$ , which leads to a gas/dust ratio around 160, with an uncertainty factor of 2.

#### 4.3. NGC 7027

NGC 7027 is known as a relatively young, carbon-rich PN composed by an ionized nebulosity and an extended halo of neutral material (e.g. Graham et al. 1993). Optical images of NGC 7027 clearly suggest the presence of dust in this nebula (Bryce et al. 1997). Several observations in other spectral ranges confirm that small solid particles at approximately 90 K coexist with the ionized gas (Bentley 1982). Moreover, this source shows millimeter and submillimeter emission excesses in the continuum (Gee et al. 1984). Some authors have pointed out the existence of, at least, two different dust components in the nebula (Kwok 1980): a warm component ( $\sim 90$  K), located at the most internal, ionized zone, and a colder component ( $\sim 20$  K), perhaps placed

in the outer neutral halo that is responsible of the millimeter and submillimeter excesses. It has been even suggested that the formation of these two components took place during different evolutive stages. The coldest dust could be associated with the most primitive remnant of the envelope ejected by the AGB star, while the 90 K dust could be formed in subsequent stages of the nebula evolution. However, up to now, no empirical data about the spatial distribution of the cold component was reported, and even its existence was only suspected.

As we have seen in Fig. 2, NGC 7027 shows a clear extended 1.3 mm emission, with a total integrated flux of approximately  $4.1 \pm 0.1$  Jy. We have considered the possible contamination of the flux by molecular line emission. From the central region of NGC 7027, where one can expect the strongest contamination, we have found a  $^{12}\text{CO}(2\text{-}1)$  flux  $\sim 0.05$  Jy. The second most intense molecular line is HCN(3-2), which contributes to the emission with a value 10 times smaller than CO. Moreover, the photospheric emission ( $T_{\text{star}} \sim 2 \cdot 10^5$  K; see for instance Jacoby 1998; Heap & Hintzen 1990) is completely negligible at this wavelength. Then, we conclude that there is no significant contribution from other emission mechanisms than free-free and dust emission. We have separated the total emission of this source in three components. First, a compact and central component that is responsible for 2.7 Jy of the total emission. After subtraction of the previous point-like component, an extended 1.4 Jy component remains (Fig. 5a). Part of the emission of this extended component seems to arise from a region at approximately  $+15''$  with a possible counterpart at  $-15''$ , in the East-West direction (approximately in the equatorial plane). The contribution to the flux of this component is about 0.3 Jy. The subtraction of such component from the total extended emission, 1.4 Jy intense, yields a  $\sim 1.1$  Jy feature elongated approximately in the axial direction. The presence of a very extended component could explain, on the other hand, the scatter in the submm observations from the literature (Fig. 5b), that would be partially due to the different spatial resolution of the observations, in such a way that smaller beams could miss the emission of the outer regions. As we will see later, the separation in two components of the total extended emission can be also understood from the spectrum of the source.

In Fig. 5b, we show the spectral energy distribution of NGC 7027. At large wavelengths, it is clear from the slope of the spectrum that the dominant mechanism of emission is free-free radiation from an HII region (dashed line). This emission has an important contribution to the flux also in the millimeter range. At smaller wavelengths (IR), thermal dust emission with temperature  $\sim 85$  K and  $\alpha \sim 2$  properly fits the spectrum (dotted line). We think that the two inner components we find at 1.3 mm continuum (2.7+1.1Jy) are due to the emission of the ionized region, since their total intensity accurately matches the extrapolated value for the free-free emission. The total flux, 4.1 Jy, does not seem to be compatible with such an extrapolation. Moreover, our map of the extended emission, excepted the 0.3 Jy component, is comparable to those obtained by Basart & Daub (1987) at 20 and 6 cm, these maps outlining free-free emission from the ionized nebula (see the sketch of the 6 cm map in Fig.

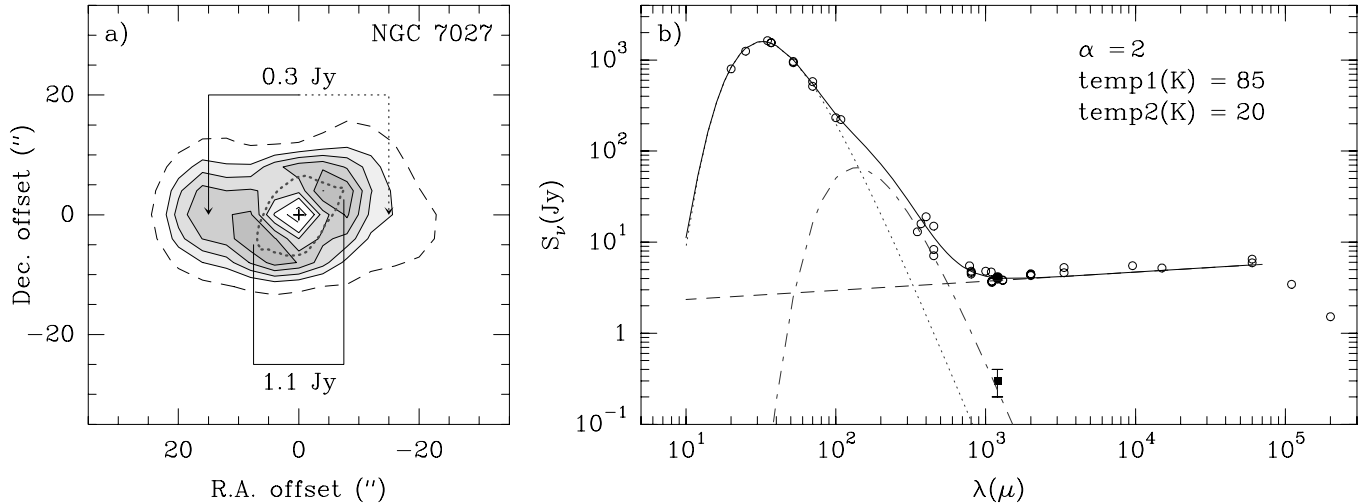


**Fig. 5.** **a** Map of the extended 1.4 Jy component of NGC 7027. Contours are 30 (dashed line) and from 50 to 100 by 12.5% of the maximum (0.27 Jy/beam). Also a sketch of the VLA 6 cm map from Basart & Daub (1987) outlining the HII region is drawn (dotted contour). **b** Spectral energy distribution of the source. We have used filled symbols to indicate our 1.3 mm data. We separately represent the total emission (circle) and the emission associated to cold dust (square) (see text Sect. 4.1). Data at other wavelengths (empty circles) are taken from: Knapp et al. (1993), Hoare et al. (1992), Altenhoff et al. (1994), Steppe et al. (1988), Gee et al. (1984), Sopka et al. (1985), Moseley (1980), Ulich (1981), Basart et al. (1987), Elias et al. (1978), Davies et al. (1967), Sandell (1994) and Sahai et al. (1989). Dashed line: optically thin free-free emission; dotted and dot-dashed lines: thermal dust emission from warm and cold components respectively; solid line: total predicted emission from our source model.

5b). The similar size and orientation of the maps supports the idea of free-free emission as the origin of the extended 3.8 Jy component. On the other hand, the differential 0.3 Jy component, that has been found to come from a region significantly more extended than the HII region, is probably not due to free-free emission. As we have previously said, there is also warm dust ( $\sim 85$  K) responsible of the IR spectrum, coexisting with the ionized gas. However, such a dust emission is extremely weak and cannot explain none of the observed components at 1.3 mm for reasonably spectral fits. In particular, the 0.3 Jy very extended component we have found at 1.3 mm wavelength cannot be due to emission by the warm dust, which is known to be confined to the ionized (inner) envelope of NGC 7027.

As we see in the spectrum of this source (Fig. 5b), the emission of the East-West component (0.3 Jy) can be explained by a cold dust component, different from the warm grains responsible for the 20-100  $\mu\text{m}$  emission. In summary, we think that we are seeing the emission from the cold dust supposed to be present in the outer halo of NGC 7027. We must remark that it is not surprising to find cold dust particles in this region. Optical images show the presence of a dust component distributed in an equatorial ring around the central star with a maximum of the grain density ( $A_v \sim 4$  mag) at approximately  $+5''$  toward the East (see for instance Bryce et al. 1997 and Robberto et al. 1993). Then, the region which emission we are seeing could be the natural extension of this ring-like structure, and it must contain colder grains due to its larger distance to the radiation source. Note that the size of the dusty region from our 1.3 mm maps ( $\sim 30''$ ) is consistent with the extent ( $\sim 44''$ ) obtained by Gee et al. (1984) from the 450  $\mu\text{m}$  emission also due to cold

dust, and with that of the CO nebula ( $\sim 70''$ , Masson et al. 1985; Bieging et al. 1991).

According to the previous discussion, we have assumed that the East-West extended component of the flux is arising from dust. Taking into account this fact, the spectral fits give us a representative temperature for cold grains of 20 K (dot-dashed line, Fig. 5b), although temperatures between 10 and 30 K are also possible. From the total spectral energy distribution, we have also found a frequency power-law exponent between 1.6 and 2.3. So, we have assumed in our calculations an average value of 2, which seems to be a frequent value in C-rich PN (Hoare et al. 1992). Note, however, that from our spectral fitting we can not exclude a different value of  $\alpha$  for the cold dust component. In fact, the supposed different stage of formation of the two dust components could explain the presence of different values of  $\alpha$ , so we have also considered  $\alpha \sim 1$  in the mass calculation.

From the analysis of the radiative equilibrium temperature of grains (Sect. 3) and assuming  $\alpha = 2$  and  $A_v \sim 3-4$  mag in the equatorial direction, we find that only grains with sizes between 1 and 20  $\mu\text{m}$  can have temperatures in the range given by the spectral fit at  $15''$  from the center. However, radii smaller than 5  $\mu\text{m}$  lead to a mass of dust excessively large ( $\sim 0.2 M_\odot$  with  $a = 1 \mu\text{m}$ ). If we assume the standard value of the gas/dust ratio for this kind of objects, about 100, then the total molecular mass of the envelope must be of the order of 20  $M_\odot$ . This high mass is not compatible with the actual ideas on the PPN evolution, which establish that the progenitor AGB star had a mass between 1 and 8  $M_\odot$ . We have finally considered particles with radii between 5 and 20  $\mu\text{m}$ . With these values we obtained a dust mass between 0.018 and 0.070  $M_\odot$ , taking also into account

the error in the flux. This value agrees with that obtained by Gee et al. ( $0.03 M_{\odot}$ ), and it is not in contradiction with the total nebular mass  $\sim 1\text{--}5 M_{\odot}$  (Knapp et al. 1982; Knapp & Morris 1985; Jaminet et al. 1991). We must recall, however, that our data do not exclude larger masses if we consider smaller grains. On the other hand, as we have mentioned, we could assume a different  $\alpha$  for cold grains. If we take  $\alpha=1$ , then the possible temperatures obtained from the spectral fit are between 40 and 20 K. To have such temperatures at  $15''$ , grains sizes must be within the interval  $\sim 0.1 - 1 \mu\text{m}$ . The mass so calculated is  $\sim 1\text{--}2 \cdot 10^{-3} M_{\odot}$ . Note, that in this case the estimated mass is specially uncertain.

We have also estimated the mass of the warm component, assuming 85 K and that it must be located in a region extended up to distances  $\lesssim 10''$  from the nebula center (Bentley et al. 1982; Moseley 1980). The latter condition constrains the grains sizes to values  $\sim 0.1 \mu\text{m}$ , resulting a value of the mass of about  $2.5 \cdot 10^{-2} M_{\odot}$ . The mass of the warm dust component has also been estimated by Telesco & Harper (1977) and McCarthy et al. (1978), which obtain values of the same order assuming grains of similar characteristics.

#### 4.4. CRL 2688

CRL 2688 is a carbon-rich PPN that shows a strong bipolar appearance in the optical (Ney et al. 1975; Sahai et al. 1998) and in the near infrared (Latter et al. 1993). In the NIR, CRL 2688 exhibits strong emission, pointing out the presence of dust in the nebula. In fact, the central star is embedded in a large obscured region in the equatorial plane, that is probably a thick disk of dust possibly ejected during the AGB phase. CRL 2688 is a reflection nebula, indicating that dust is also present in the lobes. Studies of the light scattering in the nebula (Latter et al.; Jones & Dyck 1978; Shawl & Tarengi 1976) suggest that the grains are likely to be large graphite particles. However, mid infrared images of CRL 2688 indicate the presence of an additional population of smaller grains which do not contribute to the observed scattered light.

From our mm-wave observations we have measured in CRL 2688 a total flux of  $2.1 \pm 0.1$  Jy. Also, in this case we have tried to separate the emission in two components, subtracting a compact component from the total flux. We have found that, after subtraction, the extended component is elongated along the direction of the nebula axis (see Fig. 6a) and shows a flux of about 0.3 Jy. In view of the relatively low value of the FWHM of the total emission ( $\sim 12''$ , only slightly larger than the beam size,  $11''/3$ , see Sect. 2), this extended component is only tentatively detected, its flux being very uncertain.

The spectral energy distribution of CRL 2688 is given in Fig. 6b. We find that the spectral fit at wavelengths larger than  $15 \mu\text{m}$  can be properly performed assuming a single dust component with a temperature  $\sim 115$  K. As we can see, there must be also a warmer component responsible of the emission at shorter wavelengths, that will not be discussed here. From the fitting we find for the exponent of the emissivity power-law  $\alpha \simeq 0.7$ . This low value yields to a high emissivity at radio frequencies that

has been associated to amorphous or layered carbon particles (Bussoletti et al. 1987; Rouleau & Martin 1991). Note that the relatively low value determined for  $\alpha$  can also be an effect of the presence of a radial gradient of the temperature and grain density in the nebula. These two properties should lead to a smooth slope in this spectral region. However, from the scarce existing data, particularly the poor mapping, it is not possible to unambiguously determine the temperature and density gradients in CRL 2688 which could lead to the observed spectrum (see below).

In order to estimate the dust mass in the nebula we have considered the two previous possibilities. First, we have assumed that the total 1.3 mm emission, 2.1 Jy, arises from dust at  $\sim 115$  K located in a region relatively close to the nebula center and barely resolved by our beam. The fact that the FWHM of our map is slightly larger than the beam size of the telescope indicates that the size of the dust region is somewhat extended,  $\sim 4''$ . From the theoretical temperature distribution we find that having dust with this temperature at distances  $\lesssim 2''$  of the central star is only possible if the grains have radii  $\sim 0.2 \mu\text{m}$ . In this case we have found a value of the total dust content in the nebula of  $\sim 3 \cdot 10^{-4} M_{\odot}$ .

The previous value of the dust mass is only a lower limit, since it is also possible to fit the spectrum with more components (second case), one of them colder than 100 K, which systematically leads to larger dust masses. This complex structure of the nebula is in particular supported by data at cm-wavelengths. Knapp et al. (1994) observed the radio continuum at 3.6 cm from this source, and found that the emission extended up to distances  $\sim 15''$  from the nebula center. The most likely mechanism in this spectral range is also thermal dust emission, so one can conclude that probably there are grains at large distance. The size of the dusty region in the Knapp et al.'s observations is larger than our 1.3 mm map, so we are very probably seeing different dust components. If so, the 3.6 cm map will give information on a colder dust component in the envelope which is responsible of the long wave spectrum ( $\lambda > 1.3$  cm). Taking into account this fact, we have fitted the CRL 2688 spectrum ( $\lambda < 1.3$  cm) using two different dust components. None of the spectral fits we have tried using  $\alpha = 2$  gave satisfactory results. Using a spectral index  $\alpha = 1$ , we have found a proper fit with a warm component ( $T \sim 100$  K), and a colder component, needed to reproduce the millimeter continuum excess, with temperatures below 15 K. From our 1.3 mm map, we have found that the largest distance from the center that can be reached by the extended component is  $\sim 6''$  (such a distance depends on the uncertain intensity of the subtracted point-like component). However, from the theoretical temperature distribution we find that such low temperatures are only possible if grains have sizes  $\gtrsim 1000 \mu\text{m}$ . If grains have such size then the emissivity law will be flat at wavelengths shorter than 1.3 cm. In this case, the spectrum can be properly fitted with any value of the temperature. However, a lower limit to the temperature of the grains is given by the maximal extent of our map and the theoretical temperature distribution. We find that 40 K is the lowest possible value, which yields an upper limit of the cold dust mass of  $\sim 0.015 M_{\odot}$  (using  $1000 \mu\text{m}$

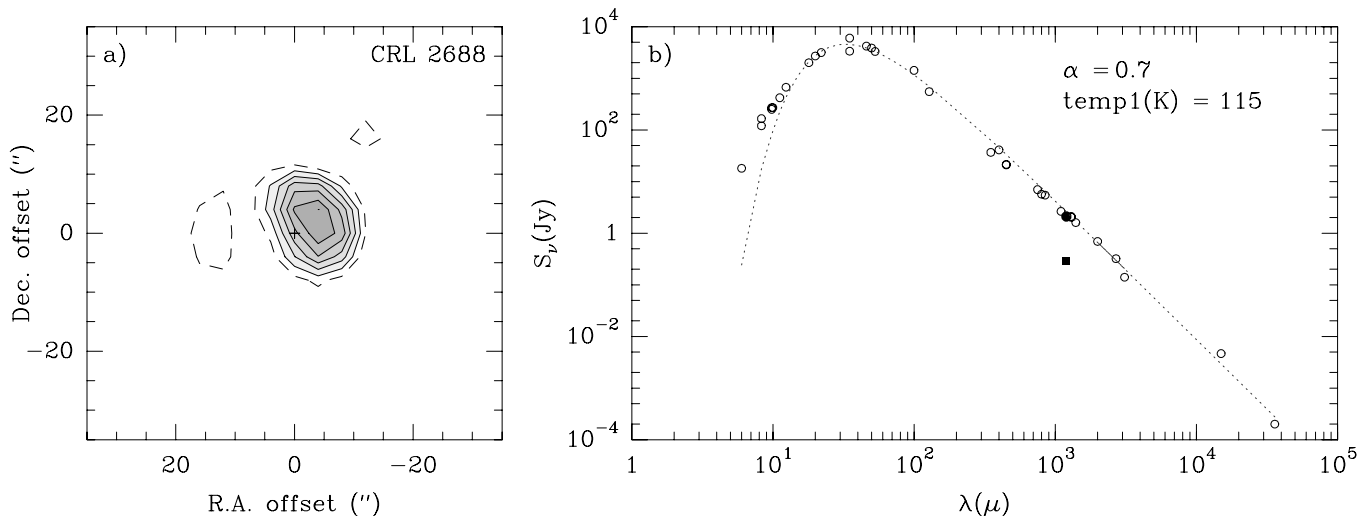


**Fig. 6.** **a** Map of the extended component of CRL 2688, Contours are 25 (dashed) and from 37.5 to 100 by 12.5% of the maximum (0.22 Jy/beam). **b** Spectral energy distribution of the source. Filled symbols represent our 1.3 mm data; the circle is the total flux and the square is a representative flux of the extended component. Empty circles are data from Knapp et al. (1993, 1994), Sopka et al. (1985), Harvey et al. (1991), Heiligman et al. (1986), Woody et al. (1989), Sahai et al. (1989), Walmsley et al. (1991), Omont et al. (1995), Yamamura et al. (1995), Kleinmann et al. (1978) and Jaye et al. (1989). Dotted line: thermal dust emission.

grains). The estimated mass of the warm dust component is in this case  $\sim 2 \cdot 10^{-3} M_{\odot}$ . The fluxes for the cold and warm dust components used in the previous estimations are directly obtained from the spectral fit.

It is remarkable the difference between the total dust mass obtained supposing a single (115 K) or two (100 K and 40 K) dust components in the nebula. This fact is due to the strong dependence of the mass calculation on the values of the grains radius and  $\alpha$ . Therefore, the estimation of the total dust mass in CRL 2688 is very uncertain, mainly due to the difficulty in estimating the cool dust component. Our average value of the dust mass is  $\sim 2 \cdot 10^{-3} M_{\odot}$ , with an error of almost a factor 10. Even if the uncertainty is high, we believe that this value is representative. It is compatible with the dust mass-loss rates estimated by several authors (Knapp et al. 1994; Yamamura et al. 1996),  $\dot{M}_{\text{dust}} \sim 1.5\text{-}2 \cdot 10^{-6} M_{\odot} \text{ yr}^{-1}$ . Taking into account the expansion velocity of the envelope,  $\sim 20 \text{ km s}^{-1}$ , and the total extent of the 3.6 cm emission, the time spent by dust to reach such distance is  $\sim 3000 \text{ yr}$ . Assuming the previous mass-loss rate, a total dust mass of  $\sim 4.5 \cdot 10^{-3} M_{\odot}$  is obtained. Our value of the mass content is also compatible with previously estimated total mass-loss rates,  $\dot{M} \sim 10^{-4} M_{\odot} \text{ yr}^{-1}$  (e.g. Knapp & Morris 1985; Morris 1980) for standard gas-to-dust mass ratios.

#### 4.5. Point-like sources

In Table 1, we can also see the 1.3 mm flux from objects with point-like appearance. We have found emission from M 1-92 and, tentatively, M 1-91, PPNe which have not been previously detected at this wavelength. For NGC 2346, R Sct and M2-56, sources without previous data at 1.3 mm, we only give upper limits to the flux. We have found a good agreement between our results and data from observations carried out by other authors

for almost all sources (Walmsley et al. 1991; Knapp et al. 1993; Altenhoff et al. 1994). For VY CMa and R Aqr there are differences between our flux and those from Walmsley et al. (who used the SEST 15m telescope for these two sources),  $\sim 378$  and  $\sim 143 \text{ mJy}$  respectively; however, our data are very similar to those of Knapp et al. and Altenhoff et al. We cannot rule out that those flux differences are intrinsic, since both sources are known to be variables.

In the case of point-like sources the estimation of the dust mass in the nebula would be still more uncertain due to the impossibility of properly establish either the different components of the observed flux and the total extent of the cold dust in the nebula.

## 5. Conclusions

We have carried out maps of the 1.3 mm continuum emission in a sample of 16 evolved stars, obtaining the following results:

a) We have found millimeter emission in 11 objects (see Table 1), among which two are new detections: M 1-92 and, tentatively, M 1-91.

b) We have found extended emission in 4 sources: M 2-9, OH 231.8+4.2, NGC 7027 and CRL 2688 (tentatively). In all these cases, we argue that at least a part of such emission is arising from relatively cold dust. From the spectral fit we have obtained dust temperatures ranging between 5 and 40 K, except for CRL 2688 for which the temperature is more uncertain and higher values are possible. Our data constitute then, the first cartography of extended 1.3 mm emission in PPNe.

c) M 2-9, OH 231.8+4.2 and CRL 2688, present extended cold dust emission elongated in the direction of the nebula axis. This fact could suggest that the dust responsible for the continuum emission at this wavelength is rather located along the

lobes than in the equatorial plane, or that the equatorial region containing dust is not resolved by our beam ( $\sim 11''$ ). We think that, in fact, it is not surprising to find dust at large distances from the star in regions showing the highest velocities, as is the case of the lobes in proto- and young planetary nebulae.

d) In NGC 7027, the extended radio continuum emission has been separated in two components. One of these, directed along the nebula axis, seem to be associated to free-free emission. The other component extends almost in the equatorial plane up to a distance of  $\sim 15''$  and, we argue, arises from cold dust. This extended component seem to outline the outer region of a torus/disk of dust observed at other spectral ranges.

e) We have performed simple model calculations assuming radiative equilibrium in an optically thin envelope in order to estimate the dust temperature at a given distance to the center. From the comparison of our data (extent of our maps, dust temperature and exponent of the emissivity power-law,  $\alpha$ ) with such a theoretical temperature distribution, we have obtained an estimation of the grain radii. We have found that grains must have sizes larger than those in the interstellar medium in order to reproduce our data, in general between  $\sim 1 - 100 \mu\text{m}$ . We must note, that our estimations are not free from uncertainties, mainly due to the difficulty of clearly separate the emission arising from cold dust and to the uncertainty in the dust emission model.

f) We have also estimated the mass of cold dust in the sources which present extended emission (see Table 2). M 2-9, OH 231.8+4.2 and CRL 2688, have cold dust masses of the order  $\sim 10^{-3} M_{\odot}$ , while NGC 7027 seems to have a greater dust content,  $\sim 10^{-2} M_{\odot}$ . The uncertainty in our mass calculations is notably high in the cases of NGC 7027 and CRL 2688: of about a factor 10. We have also estimated the mass of the warm dust component for the extended sources, and we find values always equal or smaller than those of the cold component. We accordingly conclude that a large fraction of the total dust content is in the extended cold dust component.

*Acknowledgements.* This work has been partially supported by DGES, project number PB96-0104. C. Sánchez Contreras is grateful for the support from the Universidad Complutense de Madrid, through a Complutense grant.

## References

- Allen, D. A. and Swings, J. P., 1972, *ApJ* 174, 583
- Altenhoff, W.J., Thum, C., and Wendker, H.J., 1994, *A&A* 281, 161
- Aspin, C., McLean, I. S. and Smith, M. G., 1988, *A&A* 196, 227
- Bachiller, R., Gómez-González, J., Bujarrabal, V., and Martín-Pintado, 1988, *A&A* 196, L5
- Basart, J. P. and Daub, C. T., 1987, *ApJ* 317, 412
- Beichman, C.A., Neugebauer, G., Habing, H.J., Clegg, P.E., and Chester, T.J., 1988, *Infrared Astronomical Satellite (IRAS), Catalogs and Atlases*, NASA RP-1190, US Gov. Printing Office, Washington DC
- Bentley, A.F., 1982, *AJ* 87, 1810
- Bieging, J.H., Wilner, D., and Thronson, H., 1991, *ApJ* 379, 271
- Bowers, P. F. and Knapp, G. R., 1989, *ApJ* 347, 325
- Bowers, P. F. and Morris, M., 1984, *ApJ* 276, 646
- Broguière, D., Neri, R., and Sievers, A., 1996, *NIC Bolometer User's Guide*, IRAM Document
- Bryce, M., Pedlar, T., Muxlow, T., Thomasson, P. and Mellema, G., 1997, *MNRAS* 284, 815
- Bussoletti, E., Colangeli, L., Borghesi, A. and Orofino, U., 1987, *A&AS* 70, 257
- Cohen, M., 1981, *PASP* 93, 288
- Cohen, M., Dopita, M.A., Schwartz, R.D., and Tielens, A.G.G., 1985, *ApJ* 297, 702
- Davies, J.G., Ferriday, R.J., Haslam, C.G.T., Moran, M., and Thomasson, P., 1967, *MNRAS* 135, 139
- Elias, J.H., Neugebauer, G., Werner, M. W., Ennis, D. J., Gezari, D. Y., Houck, J. R., Matthews, K., Nadeau, D., Hauser, M. G., and Lo, K. Y., 1978, *ApJ* 220, 25
- Feast, M.W., Catchpole, R.M., Whitelock, P.A., Roberts, G., Spencer Jones, J., and Carter, B.S., 1983, *MNRAS* 203, 1207
- Gee, G., Emerson, J. P., Ade, P. A. R., Robson, E.I., and Nolt, I.G., 1984, *MNRAS* 208, 517
- Gezari, D.Y., Schmitz, M., and Mead, J.M., 1987, *Catalog of Infrared Observations*, 2nd edition, NASA RP-1196
- Gilman, R.C., 1974, *ApSS* 28, 397
- Gillet, F.C., and Soifer, B.T., 1976, *ApJ* 207, 780
- Graham, J. R., Herbst, T. M., Matthews, K., Neugebauer, G., Soifer, B. T., Serabyn, E. and Beckwith, S., 1993, *ApJ* 408, L105
- Harvey, P.M., Lester, D.F., Brock, D., and Joy, M., 1991, *ApJ* 368, 558
- Heap, S. R., and Hintzen, P. 1990, *ApJ* 353, 200
- Heiligman, G.M., Berge, G. L., Claussen, M. J., Leighton, R. B., Lo, K. Y., Masson, C. R., Moffet, A. T., Phillips, T. G., Sargent, A. I., Scott, S. L., Scoville, N. Z., Wannier, P. G., and Woody, D. P., 1986, *ApJ* 308, 306
- Hildebrand, R.H., 1983, *QJRAS* 24, 283
- Hoare, M. G., Roche, P. F. and Clegg, R. E. S., 1992, *MNRAS* 258, 257
- Jacoby, G. H. 1988, *ApJ* 333, 193
- Jamiet, P.A., Danchi, W.C., Sutton, E.C., Bieging, J.H., Wilner, D., Russel, A.P.G., Sandell, G., 1991, *ApJ* 380, 461
- Jaye, D., Fienberg, R.T., Fazio, G.G., Gezari, D.Y., Lamb, G.M., Shu, P.K., Hoffmann, W.F., McCreight, C.R., 1989, *AJ* 97(3), 809
- Jones, T.J., and Dyck, H.M., 1978, *ApJ* 220, 159
- Jura, M., Turner, J., and Balm, S. P., 1997, *ApJ* 474, 741
- Kastner, J. H., and Weintraub, D. A., 1995, *AJ* 109(3), 1211
- Kastner J.H., Weintraub D.A., Zuckerman B., Becklin E.E., McLean I., Gatley I., 1992, *ApJ* 398, 552
- Kleinmann, S.G., Sargent, D.G., Moseley, H., Harper, D.A., Loewenstein, R.F., Telesco, C.M., and Thronson, H.A., 1978, *A&A* 65, 139
- Knapp, G.R., Phillips, T. G., Leighton, R. B., Lo, K. Y., Wannier, P. G., Wootten, H. A. and Huggins, P. J., 1982, *ApJ* 252, 616
- Knapp, G.R., and Morris, M., 1985, *ApJ* 292, 640
- Knapp, G.R., Sandell, G., and Robson, E.I., 1993, *ApJSS* 88, 173
- Knapp, G.R., Bowers, P.F., Young, K., and Phillips, T.G., 1994, *ApJ* 429, L33
- Knapp, G.R., Bowers, P.F., Young, K., and Phillips, T.G., 1995, *ApJ* 455, 293
- Kwok, S., 1980, *ApJ* 236, 592
- Kwok, S., Purton, C. R., Matthews, H. E., and Spoelstra, T. A. T., 1985, *A&A* 144, 321
- Kohoutek, L. & Surdej, J., 1980, *A&A* 85, 161
- Kreysa, E., 1990, *Proc.29th Liège ESA SP-314*, 265
- Latter, W.B., Hora, J.L., Kelly, D.M., Deutsch, L.K., and Maloney, P.R., 1993, *ApJ* 106(1), 260

- Leung, C.M., 1975, *ApJ* 199, 340
- McCarthy, J.F., Forrest, W.J., and Houck, J.R., 1978, *ApJ* 224, 109
- Masson, C. R., Cheung, K. W., Berge, G. L., Claussen, M. J., Heiligman, G. M., Leighton, R. B., Lo, K. Y., Moffet, A. T., Phillips, T. G., Sargent, A. I., Scott, S. L., and Woody, D. P. 1985, *ApJ* 292, 464
- Mezger, P.G., Schraml, J., and Terzian, Y., 1967, *ApJ* 150, 807
- Middlemass, D., 1990, *MNRAS* 244, 294
- Milne, D.K., and Aller, L.H., 1982, *A&AS* 50, 209
- Morris, M., 1980, *ApJ* 236, 823
- Moseley, H., 1980, *ApJ* 238, 892
- Ney, E.P., Merrill, K.M., Becklin, E.E., Neugebauer, G., and Wynn-Williams, C.G., 1975, *ApJ* 198, L129
- Omont, A., Moseley, S. H., Cox, P., Glaccum, W., Casey, S., Forveille, T., Chan, Kin-Wing, Szczerba, R., Loewenstein, R. F., Harvey, P. M., and Kwok, S., 1995, *ApJ* 454, 819
- Panagia, N. and Felli, M., 1975, *A&A* 39, 1
- Purton, C. R., Feldman, F. A. and Marsh, K. A., 1975, *ApJ* 195, 479
- Purton, C. R., Feldman, F. A., Marsh, K. A., Allen, D.A., and Wright, A.E., 1982, *MNRAS* 198, 321
- Reipurth, B., 1987, *Nature* Vol. 325, 6107, 787
- Robberto, M., Clampin, M., Ligorì, S., Paresce, F., and Staude, H. J., 1993, *A&A* 280, 241
- Rouleau, F., and Martin, P. G., 1991, *ApJ* 377, 526
- Rowan-Robinson, M., 1986, *MNRAS* 219, 737
- Sahai, R., Calussen, M.J., and Masson, C.R., 1989, *A&A* 220, 92
- Sahai, R., Trauger, J.T., Watson, A.M., Stapelfeldt, K.R., Hester, J. J., Burrows, C. J., Ballister, G. E., Clarke, J. T., Crisp, D., Evans, R. W., Gallagher, J. S. III, Griffiths, R. E., Hoessel, J. G., Holtzman, J. A., Mould, J. R., Scowen, P. A., and Westphal, J. A., 1998, *ApJ* 493, 301
- Sánchez Contreras, C., Bujarrabal, V., and Alcolea, J., 1997, *A&A* 327, 689
- Sandell, G., 1994, *MNRAS* 271, 75
- Schwartz, P.R., 1982, *ApJ* 252, 589
- Schwarz, H. E., Aspin, C., Corradi, R. L. M., and Bo Reipurth, 1997, *A&A* 319, 267
- Shawl, S.J., and Tarengi, M., 1976, *ApJ* 204, L25
- Shure, M., Sellgren, K., Jones, T.J., and Klebe, D., 1995, *AJ* 109(2), 721
- Soifer, B.T., Willner, S.P., Capps, R.W., and Rudy, R.J., 1981, *ApJ* 250, 631
- Sopka, R.J., Hildebrand, R., Jaffe, D.T., Gatley, I., Roelling, T., Werner, M., Jura, M., and Zuckerman, B., 1985, *ApJ* 294, 242,
- Steppe, H., Salter, C.J., Chini, R., Kreysa, E., Brunswig, W., and Lobato Pérez, J., 1988, *A&AS* 75, 317
- Telesco, C.M., and Harper, D.A., 1977, *ApJ* 211, 475
- Thum, C., 1992, *IRAM Working Report* 212
- Ulich, B.L., 1981, *AJ* 86, 1619
- Walmsley C.M., Chini, R., Kreysa, E., Steppe, H., Forveille, T., and Omont, A., 1991, *A&A* 248, 555
- Woodward, C.E., Forrest, W.J., Pipher, J.L., Moneti, A., and Shure, M., 1989, *ApJ* 337, 754
- Woody, D.P., Scott, S. L., Scoville, N. Z., Mundy, L. G., Sargent, A. I., Padin, S., Tinney, C. G., and Wilson, C. D., 1989, *ApJ* 337, L41
- Yamamura, I., Onaka, T, Kamijo, F., Deguchi, S., and Ukita, N., 1995, *ApJ* 439, L13
- Yamamura, I., Onaka, T, and Kamijo, F., 1996, *ApJ* 465, 926
- Zijlstra, A.A., Pottasch, S.R., and Bignell, C., 1989, *A&AS* 79(3), 329
- Zweigle, J., Neri, R., Bachiller, R., Bujarrabal, V., and Grewing, M., 1997, *A&A* 324, 624